PHYSICAL REVIEW A VOLUME 36, NUMBER 2 JULY 15, 1987

Galvanic detection of laser photoionization in hollow-cathode discharges: Experimental and theoretical study

M. Broglia, F. Catoni, A. Montone, and P. Zampetti
Comitato Nazionale per la Ricerca e per lo Sviluppo dell'Energia Nucleare e delle Energie Alternative,
Centro Ricerche Energetiche della Casaccia, Dipartimento Ciclo del Combustibile Divisione Ingegneria
Sperimentale Arricchimento, P.O. Box 2400, 00100 Roma A.D., Italy

(Received 28 February 1986; revised manuscript received 19 January 1987)

Resonant laser photoionization in hollow-cathode discharges has been detected and extensively studied. The direct charge production and the high electric field in the cathode dark space, that permits a very fast charge collection, enable us to detect a photoionization signal much faster than the conventional optogalvanic effect. A theoretical interpretation of the signal is given, supported by a very good agreement between numerical and experimental results. Detection limits of this technique are also evaluated.

I. INTRODUCTION

Resonant laser excitation of an atomic species in a hollow-cathode discharge results in a discharge impedance change that can be detected as a voltage drop across a ballast resistor in the lamp feeding circuit (optogalvanic effect).[1] Apart from some neon transitions involving excitation from metastable states,[2] usually nonionizing laser excitation enhances the discharge net ionization rates indirectly.[3] Short-pulsed laser excitation produces signals in the μs range, whose characteristic times have been ascribed to the mechanisms of perturbation and restoring of the discharge steady state.[4]

In a previous work[5] we first presented detection and discrimination of signals much faster than the conventional optogalvanic effect, and related them to some effects of direct laser photoionization. Striking evidence of the signal dependence on the laser tuning and connection with the region near the cathode walls have also been pointed out.

In this work the resonant photoionization signal in the cathode dark space has been closely examined, with special regard to its time and amplitude behaviors: two consecutive time components can be detected which are functions of the laser-beam position in the dark space. A theoretical model of the charge production and collection in the high electric field region has been worked out. The excellent agreement between experimental and theoretical results supports our interpretation of the signal as a fast charge collection. The very simple detection system and the signal independence from the complex discharge phenomena involving optogalvanic effects, encourages investigation of this technique for new spectroscopic and analytical applications.

II. EXPERIMENTAL SETUP

The experimental setup we have used to induce and detect photoionization in hollow-cathode discharges is shown in Fig. 1. The third harmonic from a Nd-YAG laser (where YAG represents yttrium aluminum garnet) is used to pump a dye laser and obtain tunable radiation in the 4000-Å region, with a spectral bandwidth of about 10 GHz. A second dye laser can be eventually pumped by the same Nd-YAG laser for two-step photoionization experiments. Typical peak powers are in the 10-kW range with a pulse duration of about 6 ns as measured by a vacuum photodiode (rise time 500 ps). The laser beam is focused into a U-Ne commercial hollow-cathode lamp, parallel to the cathode axis (beam cross section ~0.01 mm^2), and photoionization signals are detected across a 50-Ω ballast resistor on the grounded electrode. The circuitry time response can be evaluated by estimating the lamp parasitic capacities. The measured capacity between the electrode pins in the switched-off lamp is about 6 pF. When the lamp is switched on, the cathode dark-space limit can be considered as an effective anode (this will be described later); from geometrical considerations, a parasitic capacity of about 2–3 pF is calculated, leading to a total capacity less than 10 pF, i.e., a time constant less than 0.5 ns. The fast amplifier (ORTEC 9301), finally, yields a total time constant of about 1 ns. The photoionization signal can be time or amplitude analyzed by a fast transient digitizer (and PDP11/34 minicomputer) or a boxcar averager, respectively.

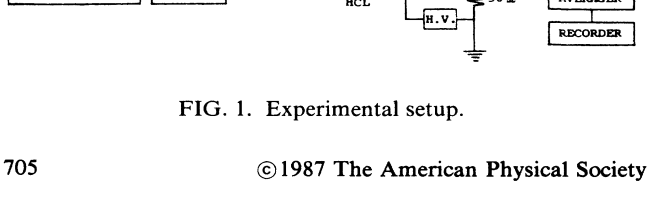

FIG. 1. Experimental setup.

III. EXPERIMENTAL RESULTS

In Ref. 5 we demonstrated the correspondence between our direct charge production in the discharge and the appearance of a signal as fast as the laser pulse. In order to exclude all possibility of spurious effects due to the cathode bottom (laser ablation, photoelectric effect, etc.), all the experimental findings characterizing the photoionization signal have been verified with two-step resonant ionization of Ne $^3P_2(1s_5)$ in a see-through In-Ne commercial hollow-cathode lamp (see Fig. 2).

Figure 3 shows the specific uranium photoionization scheme we have used in the present work. A linear dependence of the signal amplitude on laser intensity has already been reported for this interaction scheme.[5] A generally strong enhancement of photoionization signals near the cathode walls have also been noted.[5]

Typical photoionization signals near the walls are shown in Fig. 4. Both circuit configurations shown in the figure (cathode and anode signal detection) have been checked, obtaining identical, but opposite, fast signals. In the signal profile we note two time components: the first one as fast as the laser pulse, and a second slower and less intense one. A strict characterization of the time profile of the faster component is given in Fig. 5, where the single shot signal and the laser pulse (photodiode signal) that produced it appear to be nearly identical.

The time and amplitude behaviors of the photoionization signal, as a function of different positions in the discharge, have been investigated by shifting the lamp parallel to the laser beam. In Fig. 6 the fast signal amplitude is given as a function of the laser-beam position. The better spatial resolution of this measurement, compared to the first experimental results reported in Ref. 5 allowed us to connect the fast signal detection with the cathode dark space that extends very close to the cathode

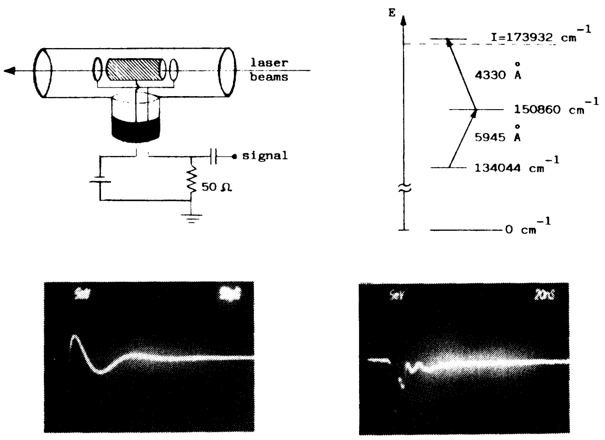

FIG. 2. Detected electrical signal produced by two-step resonant photoionization of Ne$^3P_2(1s_5)$ in a see-through hollow-cathode discharge. The optogalvanic effect related to the first step (5945 Å) is visible in the μs range; when the second laser is switched on and tuned on an autoionizing state, a mere expansion of the oscilloscope time scale makes the fast photoionization signal evident. This signal is strictly dependent on both lasers tuning and strongly enhanced near the cathode walls.

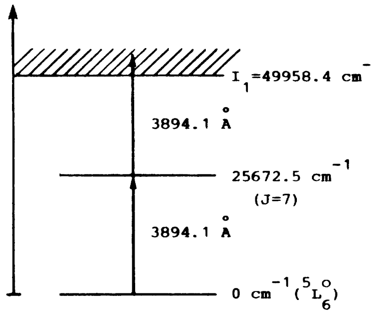

FIG. 3. Resonant two-photon ionization scheme for atomic uranium.

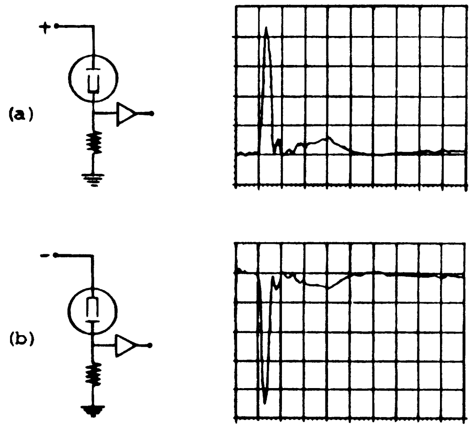

FIG. 4. Photoionization signal detection (a) on the cathode and (b) on the anode. Reported signals are averages over 100 laser pulses. Horizontal scale, 20 ns/div; vertical scale, 5 mV/div.

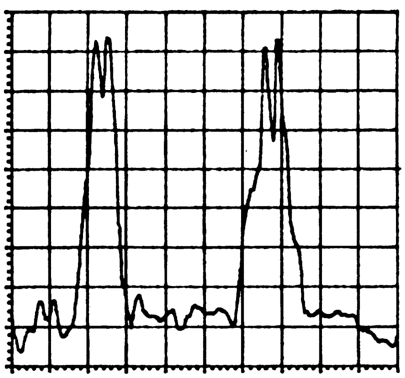

FIG. 5. Simultaneous single shot acquisition of (a) one photoionization signal (fast part) and (b) the laser pulse producing it (for visual facility the latter signal has been suitably delayed). Time scale, 10 ns/div.

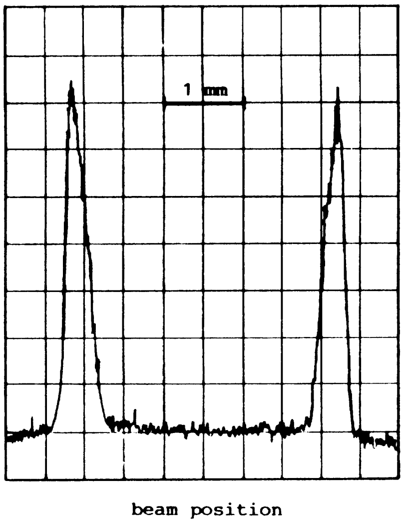

FIG. 6. Relative intensity of the photoionization signal vs beam position inside the cathode (working current 2.5 mA).

surface.[6] Indeed, a higher working current in the lamp, reducing the dark-space thickness, produces profiles similar to Fig. 6 with narrower side peaks.

Also, the time behavior of the signal for different beam positions in the dark space has been closely examined. The signal sequence shown in Fig. 7 has been obtained shifting the cathode wall away from the beam. It should be noted that the intensity of the fast signal decreases and the slower peak moves to longer times.

IV. THEORETICAL MODELS

In order to investigate the potential uses of photoionization in hollow-cathode discharges, we must know how produced charges give rise to the electrically detected signal. Our experimental results seem to suggest a fast charge collection on the electrodes because of the high electric field which characterizes the cathode dark space. In order to check this hypothesis, a modeling of charge production and collection in this region has been performed.

Our experimental conditions are shown in Fig. 8. The hollow-cathode discharge is a special glow discharge which presents only two main regions: the cathode dark space and the negative glow. The cathode dark space is a thin region (less than 0.5 mm thick[7]) very close to the cathode internal surface, characterized by a net positive space charge and a very high electric field. Nearly all the cathode voltage fall is dropped in this region, where a linear field distribution has been always experimentally found.[6,8] The negative glow extends as far as the anode. It is characterized by an almost-neutral plasma and it is nearly entirely field-free, like an electric conductor. As a consequence of this, the dark-space limit has the same potential as the anode and we can consider it an "effective" anode.

In our modeling we consider production and motion of charges in the dark space only, where we can detect the most intense photoionization signal. In a first approximation we shall consider a nonperturbation case in which the laser-produced charge densities are much less than the steady-state charge densities in the dark space. In this approximation we can model the dark space with a linearly decreasing electric field in which our charges start at rest

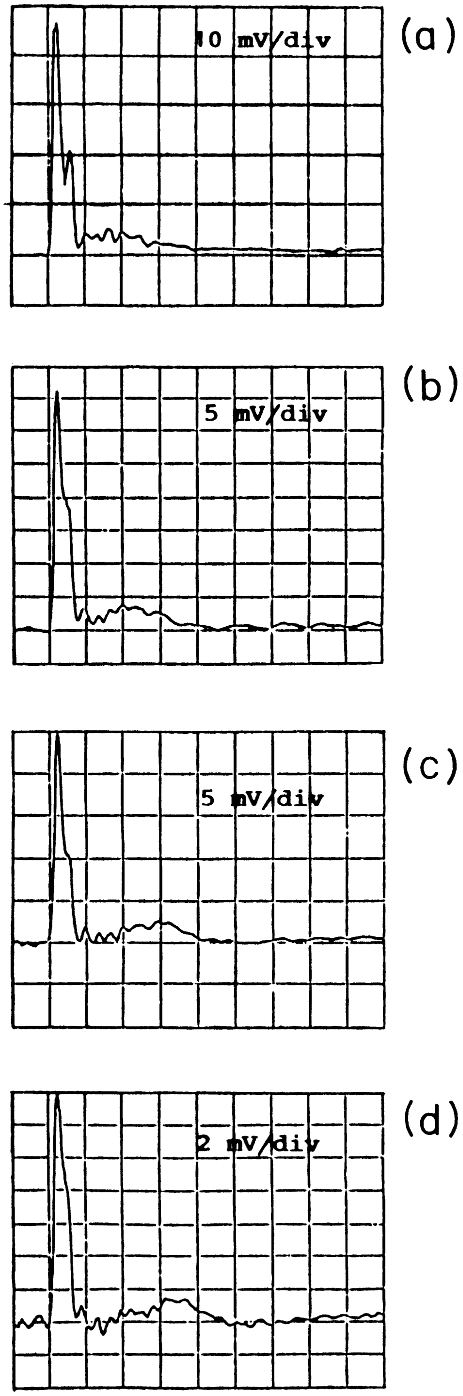

FIG. 7. Time behavior of the photoionization signal in the cathode dark space for increasing distances of the cathode wall from the laser beam. Time scale, 20 ns/div.

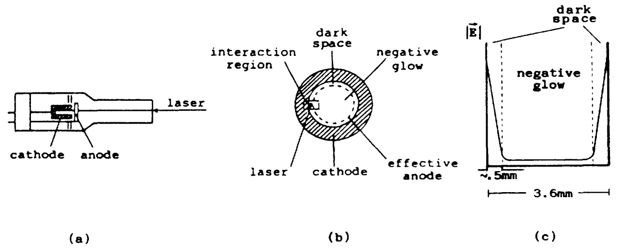

FIG. 8. Basic geometrical conditions for the theoretical models. (a) Hollow-cathode lamp and laser irradiation, (b) cross section of the cathode and discharge regions, and (c) electric field distribution across a cathode diameter.

and move as point charges without any self-induced effects. Later on we will try a more general treatment in which building and perturbation of the steady-state conditions are considered and will support a quantitative evaluation of sensitivity of this technique.

A. Point-charge model

As we emphasized, we detect photoionization signals in the same time range as the laser pulses we use to produce them. Therefore, in order to reconstruct the whole timing of the signals we must convolve production and collection of charges.

The interaction process shown in Fig. 3 is a resonant two-photon photoionization process of atomic uranium: one photon excites uranium into the 25 672.465-cm^{-1} level[9] and a second one, from the same laser, ionizes the excited atoms. Usually, ionization cross sections are 2—3 orders of magnitude smaller than resonant absorption cross sections.[10] In a wide range of laser power, the simplest "rate equation" model for this process[10] involves saturation of the first transition and then a linear dependence of the photoionization rate on laser intensity can be assumed. In our power range, this assumption seems to be supported by the experimental results reported in Ref. 5. Therefore, for our model, we consider a production rate of charge density:

$$\frac{\partial n_{e,i}(x,t)}{\partial t}=KI(x,t)\ , \tag{1}$$

where n_e and n_i are electron and ion densities, respectively. For numerical purposes, a space-time Gaussian distribution of the laser intensity has been considered:

$$I(x,t)=\frac{I_{\text{tot}}}{\pi\Delta x\,\Delta t}e^{-[(x-x_r)/(\Delta x)]^2}e^{-[(t-t_r)/(\Delta t)]^2}\ . \tag{2}$$

Due to different velocities of ions and electrons, the linear field distribution in the dark space can be caused by a uniform net positive space charge. Indeed, from the Poisson's equation and the applied potential we have

$$\frac{dE(x)}{dt}=\frac{e}{\epsilon_0}(n_i^s-n_e^s)\ , \tag{3a}$$

$$\int_0^d E(x)dx=-V_0\ , \tag{3b}$$

$$E(x)=-\frac{2V_0}{d}\left[1-\frac{x}{d}\right]\ , \tag{3c}$$

where e is the electron charge, V_0 is the applied potential (both absolute values), ϵ_0 is the permittivity of free space, d is the distance between cathode and effective anode (see Fig. 9), and n_e^s and n_i^s are the steady-space charge densities.

The electric field in Eq. (3c) drives the laser-produced electrons and ions to the electrodes, according to the equations of motion

$$\frac{dv_e(x,t)}{dt}=-\frac{e}{m}E(x)-\beta_e v_e(x,t)\ , \tag{4a}$$

$$\frac{dv_i(x,t)}{dt}=\frac{e}{M}E(x)-\beta_i v_i(x,t)\ , \tag{4b}$$

where m,β_e and M,β_i are mass and collision frequency for electrons and ions, respectively.

In order to predict the induced current signal let us start from the principle of conservation of energy;[11] i.e., the work accomplished by the electric field on the charges must equal the energy delivered by the voltage supply. That is to say, per unit time

$$iV_0=e\int_A \mathbf{E}_0(n_i\mathbf{v}_i-n_e\mathbf{v}_e)dA\ , \tag{5}$$

where $\mathbf{E}_0$ is the electric field due to the voltage difference V_0, without considering space charges, $\mathbf{v}_e$ and $\mathbf{v}_i$ are electron and ion velocities, respectively, A is the volume between cathode and anode where charges are moving, and i is the current signal.

In the balance (5) we have not included the electrostatic energy variation and the work performed on the charges by the space-charge electric field because they are mutually canceled as shown in Ref. 11. However, it should be noted that only the external applied electric field expressly appears in Eq. (5), while the local electric field, including space charge, affects charge velocities.

Two basic principles of induction are also contained in Eq. (5): no current can be induced during a charge production until charges can be considered at rest, but

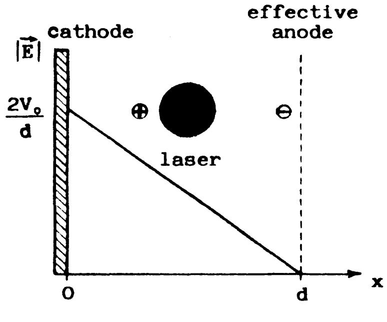

FIG. 9. Basic assumptions for the point-charge model. The dark space in the discharge steady state is simulated by a linearly decreasing electric field due to a uniform net positive space charge. The laser photoionization effect is supposed to produce charge densities much less than the steadily present ones, so that no distortion of this field has to be considered.

charges must not necessarily arrive at the electrodes, in order that a current signal can be detected in the circuit.

If we consider a theoretical plane parallel geometry, we can write

$$jV_0=\frac{eV_0}{d}\int_0^d (n_i v_i - n_e v_e)dx\ , \tag{6}$$

where motion in the direction of the field (x) alone is assumed; moreover, the current density j has been introduced to take into account the cross-section area of the interaction region.

In order to obtain the signal profile $j=j(t)$ from Eq. (6), we must be able to calculate density and velocity of charges as a function of x and t. Furthermore, in the most general case, charges with different values of velocity may be present in a given x position, at the same time t, so that the integral in Eq. (6) is replaced by a sum over all charged particles.

From Eqs. (4) we obtain velocities and positions which are functions of x_0 and $t-t_0$, where x_0 and t_0 are starting space-time coordinates of produced charges. Full expressions for v and x are

$$v_e=e^{-(\beta_e/2)(t-t_0)}(x_0-d)\left[-\frac{\beta_e^2}{2\alpha}-\frac{\alpha}{2}\right]\times\sin\left[\frac{\alpha}{2}(t-t_0)\right]\ , \tag{7}$$

$$x_e=d+e^{-(\beta_e/2)(t-t_0)}(x_0-d)\times\left[\cos\left[\frac{\alpha}{2}(t-t_0)\right]+\frac{\beta_e}{\alpha}\sin\left[\frac{\alpha}{2}(t-t_0)\right]\right]\ , \tag{8}$$

where $\alpha=(4A_e-\beta_e^2)^{1/2}$ and $A_e=2eV_0/md^2$,

$$v_i=e^{\alpha_1(t-t_0)}\alpha_1\frac{x_0-d}{1-\frac{\alpha_1}{\alpha_2}}(1-e^{(\alpha_2-\alpha_1)(t-t_0)})\ , \tag{9}$$

$$x_i=d+e^{\alpha_1(t-t_0)}\frac{x_0-d}{1-\frac{\alpha_1}{\alpha_2}}\left[1-\frac{\alpha_1}{\alpha_2}e^{(\alpha_2-\alpha_1)(t-t_0)}\right]\ , \tag{10}$$

where

$$\alpha_{1,2}=\frac{-\beta_i\pm(\beta_i^2+4A_i)^{1/2}}{2}$$

and $A_i=2eV_0/Md^2$.

From Eq. (1) the number of electrical particles produced at x_0 to x_0+dx_0 in time t_0 to t_0+dt_0 are

$$S\,dn_{e,i}(x_0,t_0)dx_0=SKI(x_0,t_0)dx_0dt_0\ , \tag{11}$$

where S is the cross-section area of the interaction region. At time t these charges will be at $x_{e,i}$ and will have velocities $v_{e,i}$ which are given from Eqs. (7)–(10). Therefore, they will contribute to the current density with

$$dj_{e,i}(t)=\mp\frac{e}{d}[KI(x_0,t_0)dx_0dt_0]v_{e,i}(x_0,t-t_0) \tag{12}$$

(where $-$ and $+$ signs on the right-hand side are meant for electrons and ions, respectively).

The total current density is obtained by integration over all possible x_0 and t_0 values:

$$j_{e,i}(t)=\mp\int_{x_0}\int_{t_0}KI(x_0,t_0)v_{e,i}(x_0,t-t_0)dt_0dx_0 \tag{13}$$

and

$$j(t)=j_e(t)+j_i(t)\ . \tag{14}$$

Some care must be taken in setting the integration limits for the double integrals in Eq. (13). In fact, at each instant t, all and only the particles which are moving between the electrodes have to be considered; as we shall see, this could compel us to express one limit as a function of the other one. Let us consider electrons at first, and let us suppose to extend integration for x_0 to the whole range 0—d. For each x_0 value, only electrons which are not yet collected have to be counted, i.e., only t_0 values such that

$$0\le t_0\le t \quad \text{if } t<t_e^c\ , \tag{15a}$$

$$t-t_e^c\le t_0\le t \quad \text{if } t>t_e^c \tag{15b}$$

have to be considered. The collection time t_e^c of electrons on the anode is obtained from Eq. (8) for $x=d$ and results:

$$t_e^c=\frac{2}{\alpha}\left[\pi-\arctan\frac{\alpha}{\beta_e}\right] \tag{16}$$

independent of x_0.

The same procedure for ions would give t_i^c as an implicit function of x_0. Therefore, we can extend integration for t_0 to the whole range 0—t, and consider only x_0 values such that ions produced at x_0 at time t_0 have not yet attained the cathode at time t. In that case we have

$$d-x_i^c\le x_0\le d\ , \tag{17}$$

where

$$x_i^c=\frac{\alpha_2-\alpha_1}{\alpha_2e^{\alpha_1(t-t_0)}-\alpha_1e^{\alpha_2(t-t_0)}} \tag{18}$$

dependent on $(t-t_0)$.

In summary, for a space-time Gaussian laser beam, full expressions of $j_e(t)$ and $j_i(t)$ are

$$j_e(t)=\frac{KI_{\text{tot}}}{\pi\Delta x\Delta t}\frac{e}{2d}\frac{\alpha^2+\beta_e^2}{\alpha}\int_0^d\int_{0,t-t_e^c}^{t}e^{-[(x_0-x_r)/(\Delta x)]^2}e^{-[(t_0-t_r)/(\Delta t)]^2}(x_0-d)e^{-(\beta_e/2)(t-t_0)}\sin\left[\frac{\alpha}{2}(t-t_0)\right]dt_0dx_0\ , \tag{19}$$

$$j_i(t)=\frac{KI_{\text{tot}}}{\pi\Delta x\Delta t}\frac{e}{d}\frac{\alpha_1\alpha_2}{\alpha_2-\alpha_1}\int_0^t\int_{d-x_i^c}^{d}e^{-[(x_0-x_r)/(\Delta x)]^2}e^{-[(t_0-t_r)/(\Delta t)]^2}(x_0-d)e^{\alpha_1(t-t_0)}(1-e^{(\alpha_2-\alpha_1)(t-t_0)})dx_0dt_0\ . \tag{20}$$

Numerical integration of Eqs. (19) and (20), to obtain theoretical induced current signals, requires the following input parameters:

$$V_0,\ d,\ \beta_e,\ \beta_i,\ \Delta x,\ \Delta t\ .$$

The KI_{tot} parameter, proportional to the total number of produced charges, only appears as a multiplication factor and does not affect the signal time behavior. Nevertheless, it should be noted that this whole theoretical model is strictly based on a nonperturbation condition, thus it holds for a number of created charges much smaller than the steady-space charge (10^{10}—10^{11} cm^{-3}).

As far as the sign convention is concerned, we note that because of our positive x direction, which we assumed as opposite to the electric field, the resulting current is negative. Then, the induced current direction is the same as the discharge steady current and results in a voltage signal positive on the cathode and negative on the anode, as we found experimentally (Fig. 4).

Figures 10—12 show theoretical results obtained for a realistic set of parameters we have estimated from experimental or reported data.[7] Similar to Fig. 7, the sequence in Fig. 10 has been obtained by increasing the laser position distance (x_r) from the cathode wall. The basic behaviors of the fast and slow parts of the signals show a very good agreement between theoretical and experimental results. In fact, on approaching the effective anode, the fast part of the signal decreases and the slower part is spread on a longer time range, as expected.

Due to the very short time spent by electrons in the dark space before being collected on the effective anode, the fast part of the signal theoretically is resolved enough to show the laser pulse structure. Figure 11 (like Fig. 5) shows comparison between a theoretical structured laser pulse and the corresponding fast part of the current signal; no circuit integration has been included in these calculations.

The next figure (Fig. 12) is a numerical simulation of the measurement reported in Fig. 6. In that case, the gate of a boxcar integrator was put on the fast part of the photoionization signal, so that basically the electron current contribution alone was integrated. Time integration of Eq. (19) will give

$$s(x_r) \propto \int_0^d e^{-[(x_0-x_r)/(\Delta x)]^2}(x_0-d)\,dx_0\ . \qquad (21)$$

Figure 12 reports a plot of calculated $s(x_r)$ to be compared with the left half of Fig. 6. This last excellent agreement is a further positive test of our model.

B. Extended model

In the most general case, all charges which are present in the laser-discharge interaction region should be included in the Poisson's equation [Eq. (3a) to have, at each instant, the effective electric field distribution that, in turn, shifts any present charge (self-Coulombic effect)]. Therefore, an iterative and self-consistent treatment has to be developed. In our previous model we assumed not to perturb significantly the discharge: then we disregarded the laser-produced charge densities with respect to the steadily present ones. We shall approach now the matter from a more general point of view that allows us to consider the system perturbations and estimate limits of sensitivity of our technique.

A thoroughly correct model would require the possibility of dealing with all phenomena and mechanisms which initiate and sustain the whole discharge. Unfortunately, the generally up to date knowledge of glow discharges[12] still needs much theoretical and experimental investigation. Nevertheless, for our purposes, a simulation as exact as possible of buildup and properties of the cathode dark space alone could be considered satisfactory.

In order to do this, by using the discharge parameters,

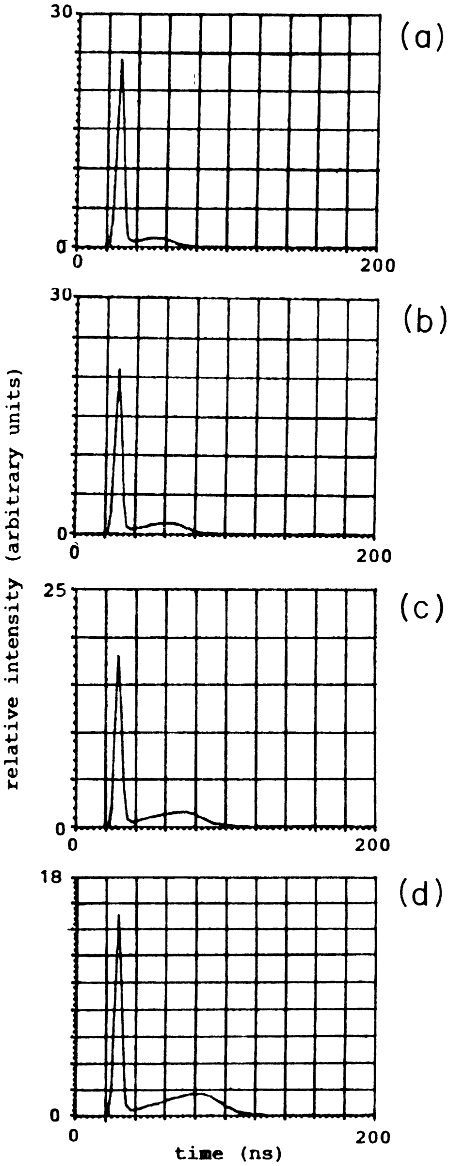

FIG. 10. Theoretical photoionization signals for different positions of the laser beam in the cathode dark space. Parameters: $V_0=200$ V; $d=0.05$ cm; $\beta_e=2$ ns^{-1}; $\beta_i=3\times10^{-2}$ ns^{-1}; $\Delta x=0.005$ cm; $\Delta t=3$ ns. From top to bottom: $x_r=0.010$, 0.015, 0.020, and 0.025 cm.

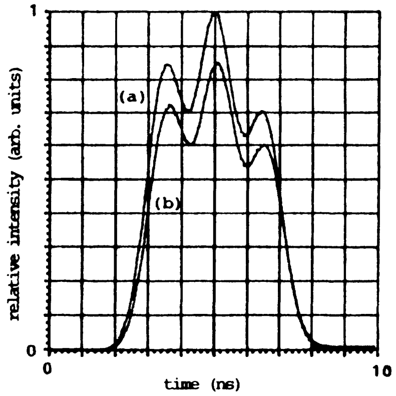

FIG. 11. (a) Theoretical laser pulse and (b) fast part of the corresponding photoionization signal. The parameters are the same as for Fig. 10; $x_r = 0.025$ cm.

we solved all the equations of balance in a hypothetical plane-parallel ionization chamber where a continuous and uniform ionization rate produces the same steady-state conditions as our discharge (Fig. 13). As we shall see, in spite of its apparent naiveté, this picture well interprets all the experimental findings with a, somewhere surprising, very good agreement.

This theoretical part is very similar to the treatment developed by Schenck *et al.* in Ref. 13 and shared by Berthoud *et al.* in Ref. 14 for the mechanism of detection of laser enhanced ionization in flames.

The modeling consists of the self-consistent and iterative solution of the continuity equations for charge densities $n_{e,i}(x,t)$ and the Poisson's equation for the electric field intensity **E**, with the external condition of the applied potential V_0. All the equations are here reported:

$$\frac{\partial n_{e,i}(x,t)}{\partial t} = -\frac{\partial F_{e,i}(x,t)}{\partial x} + r_c - \alpha n_e(x,t) n_i(x,t) + KI(x,t) , \qquad (22)$$

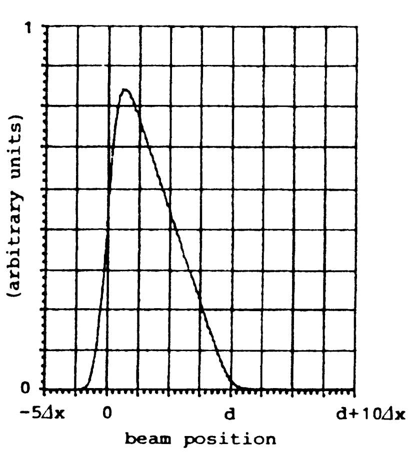

FIG. 12. Theoretical behavior of the fast signal intensity as a function of the laser position in the dark space. The parameters are the same as for Fig. 10.

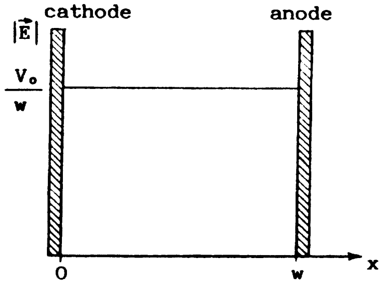

FIG. 13. Hypothetical plane-parallel ionization chamber for picture of buildup and perturbation of the dark-space steady state. In this case the discharge will be simulated as a continuous and uniform ionization rate (r_c) such that the same steady-state configuration as the discharge will be attained.

$$\frac{\partial E(x,t)}{\partial x} = \frac{e}{\epsilon_0}[n_i(x,t) - n_e(x,t)] , \qquad (23)$$

$$\int_0^w E(x,t)dx = -V_0 \qquad (24)$$

with

$$F_e(x,t) = -\mu_e E(x,t) n_e(x,t) - D_e \frac{\partial n_e(x,t)}{\partial x} , \qquad (25a)$$

$$F_i(x,t) = \mu_i E(x,t) n_i(x,t) - D_i \frac{\partial n_i(x,t)}{\partial x} , \qquad (25b)$$

and where $F_{e,i}(x,t)$ are charge fluxes ($\mathrm{cm}^{-2}\,\mathrm{s}^{-1}$), $\mu_{e,i}$ are mobilities ($\mathrm{cm}^2\,\mathrm{V}^{-1}\,\mathrm{s}^{-1}$), and $D_{e,i}$ are diffusion coefficients ($\mathrm{cm}^2\,\mathrm{s}^{-1}$) for electrons and ions, respectively; r_c is the discharge continuous ionization rate ($\mathrm{cm}^{-3}\,\mathrm{s}^{-1}$) and α is the recombination coefficient ($\mathrm{cm}^3\,\mathrm{s}^{-1}$); w is the distance between the electrodes (cm).

First of all, without laser irradiation [$I(x,t) = 0$], we set $\partial n_e/\partial t = \partial n_i/\partial t = 0$ and seek the self-consistent steady-state solution for n_e, n_i, and E. These conditions are used as a starting point for the iterative solution of Eqs. (22)–(24) when the laser pulse is switched on [introducing Eq. (2) in Eq. (22)]; the numerical solution is driven on the time scale, with suitable time steps, until restoring of the steady-state conditions.

In this case from the principle of conservation of energy the current density is given by

$$j(t) = \frac{e}{w} \int_0^w [F_i(x,t) - F_e(x,t)] dx \qquad (26)$$

(see also the Appendix).

The numerical procedure asks for the following input parameters: $V_0, w, \mu_e, \mu_i, r_c, \alpha, D_e, D_i$. As we stated earlier the first goal of this model is to attain a steady-state configuration for charge densities and electric fields as similar as possible to the dark space in the hollow-cathode discharge. That is to say, in our case, by applying 200 V between the electrodes we must obtain a nonsaturated field distribution with a 0.05-cm-thick space-charge region (sheath). Applied voltage (V_0), saturation voltage (V_s), and sheath thickness (d) are connected by[15]

$$d = \left[\frac{2V_0}{\delta} \right]^{1/2} , \qquad (27a)$$

$$V_s = \tfrac{1}{2} w^2 \delta \, , \tag{27b}$$

where

$$\delta = \left[\frac{r_c e}{\mu_i \epsilon_0} \right]^{1/2} . \tag{27c}$$

With $V_0 = 200$ V, $d = 0.05$ cm, and $r_c = 10^{18}$ cm^{-3}s^{-1} (a typical value for hollow-cathode discharges[7]), we obtained $\mu_i = 70$ cm^{2}V^{-1}s^{-1}; a mobility 3 orders of magnitude greater has been assumed for electrons.

Moreover, a w value must be chosen such that $V_0 < V_s$ (for instance $w = 0.1$ cm, $V_s = 800$ V). Of course the w parameter, which is the distance between plane-parallel electrodes of our hypothetical ionization chamber, does not have any correspondence in our real system. Nevertheless, this is uninfluential for our purposes; in fact, as proposed by Schenck *et al.*, the signal time behavior does not depend on the real anode position but almost entirely on the sheath limit (effective anode). This occurrence [easily checked numerically by changing w to d in Eq. (26)] credits some rigor to our simulation of the dark space by a plane-parallel ionization chamber. At the same time, without any logical discrepancy but for physical consistency of the numerical model, we can endow the inexistent anode with a flux of secondary electron emission ($\eta = 10^{21}$ cm^{-2}s^{-1}).

Finally, the order of magnitude for α, D_e, and D_i ($\alpha = 10^{-10}$ cm^{3}s^{-1}, $D_e = 2\times10^5$ cm^{2}s^{-1}, and $D_i = 2\times10^2$ cm^{2}s^{-1}) has been deduced from characteristic times of recombination and diffusion phenomena in the discharge.[7]

We reported in Fig. 14 the steady-state configuration obtained with these values of parameters (convergence factor $\varepsilon = 10^{-3}$). These distributions come well up to our expectations about charge densities and fields in the cathode dark space, and even the calculated steady current intensity ($S \simeq 1.8$ cm^2) is consistent with typically used working conditions.

On this steady state we switch the photoionization pulse on with the following laser parameters:

$$KI_{\text{tot}} = 5\times10^8 \text{ cm}^{-2}, \quad \Delta t = 3 \text{ ns}, \quad \Delta x = 5\times10^{-3} \text{ cm} \, ,$$

$$t_r = 25 \text{ ns}, \quad x_r = 0.010, 0.015, 0.020, 0.025 \text{ cm} \, ,$$

and obtain the sequence shown in Fig. 15 which confirms the previously obtained agreement between theoretical and experimental signal behaviors.

Further information is achievable when we try to compare our two theoretical models, applying the general model to a nonperturbation particular case. In fact, theoretical current signals obtained by the extended model exhibit a "numerical noise" which depends on the convergence factor ε we accepted in the steady-state calculation and, just like the real noise, limits our signal detection possibilities.

The theoretical and experimental noise analysis of the discharge should hence be very interesting,[16] but it is not the aim of this paper. For our purposes we filtered out the highest frequencies of the numerical noise, convolving the calculated current signal ($f(\tau)$) with the Green's function of our experimental circuit:

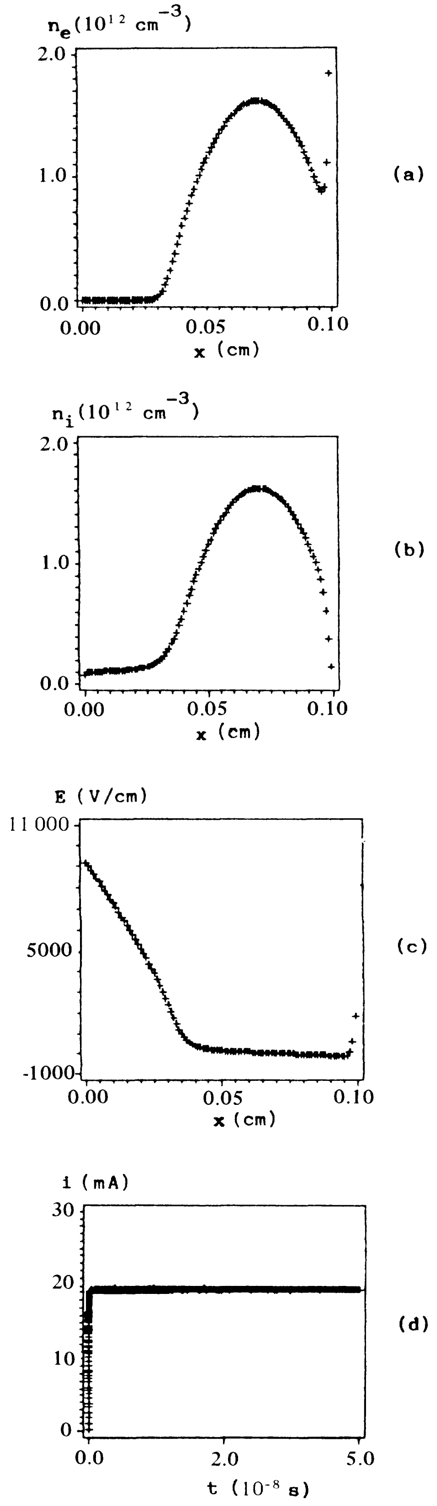

FIG. 14. Steady-state distributions for charge densities [(a) and (b)] and electric field intensity (c), obtained by numerical self-consistent solution ($\varepsilon = 10^{-3}$) of the continuity equations (with $\partial n_e/\partial t = \partial n_i/\partial t = 0$) and the Poisson's equation [Eqs. (22)–(24)]. The iterative solution of the system with the (a), (b) and (c) distributions as initial conditions and $I(x,t) = 0$ gives the steady current intensity (d). Parameters: see text.

$$s(t)=\frac{1}{T}\int_0^t e^{-(t-\tau)/T}f(\tau)d\tau\ , \tag{28}$$

where $s(t)$ is now the filtered signal and $T=1$ ns is the circuitry time constant. After that, the numerical detection limit (with $\varepsilon=10^{-3}$) is 10^5-10^6 created charges in the total dark-space volume (see Fig. 16).

On the other hand, in order to evaluate the minimum detectable signal we must take into account system fluctuations in the time duration of the gating system we use to acquire the faster and more intense signal component. Let us consider, for instance, a 20 mA working current, about $n=1.3\times10^9$ electric charges are getting to the cathode surface in a 10 ns gate width, with $\sqrt{n}=3.5\times10^4$ charge fluctuations, corresponding to a 3×10^{-2} mV (50Ω) theoretical noise. Therefore, as the faster part of the signal is proportional to one-half of the collected charges,[11] we can detect a produced charge density greater than 10^6 ions cm^{-3} in the total dark-space volume (about 7×10^{-2} cm^3). If 10^{12} cm^{-3} is the total atomic density sputtered in the discharge, we could arrange for a detection sensitivity of 10^{-6}. In our present experimental setup the intrinsic electric noise of the fast amplifier (0.1 mV) limits our detection possibility.

In our opinion, this numerous set of agreements be-

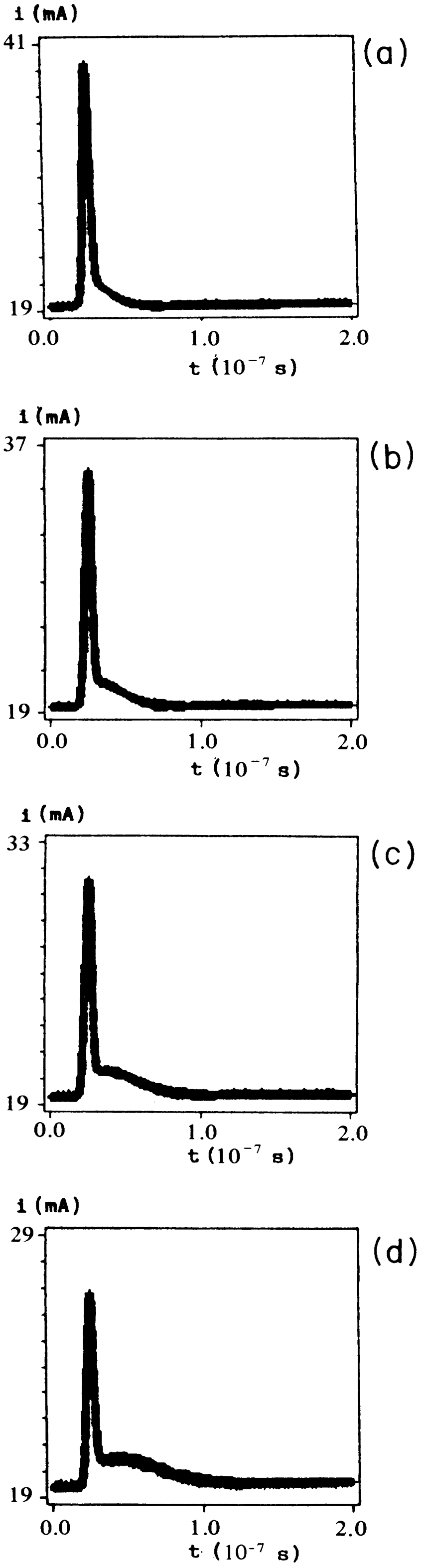

FIG. 15. Theoretical photoionization signals for different laser positions in the high electric field region of the steady state reported in Fig. 14. From top to bottom the laser beam is shifted away from the cathode wall. Parameters: see text.

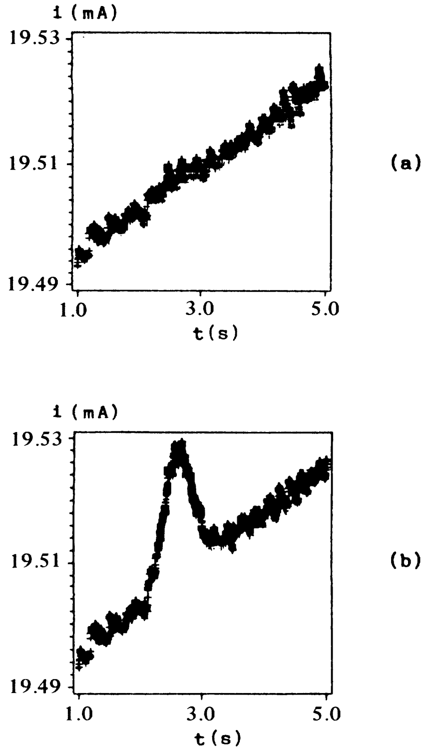

FIG. 16. Numerical signal detection limit; the steady-state starting conditions are the same as Fig. 14 ($\varepsilon=10^{-3}$). Laser-beam parameters: $t_r=25$ ns; $\Delta t=3$ ns; $x_r=0.020$ cm; $\Delta x=0.010$ cm; (a) $KI_{\text{tot}}=10^5$ cm^{-2}; (b) $KI_{\text{tot}}=10^6$ cm^{-2}; in these plots the strong expansion of the vertical scale stresses the increasing behavior due to the exponential function we use to filter the numerical noise.

tween theory and experiments proves that laser photoionization can be investigated in the cathode dark space of a glow discharge just as we do in the space-charge region of a plane-parallel ionization chamber. This endows photoionization and most of its applications with a new powerful experimental technique.

V. CONCLUSIONS

The photoionization signal in the cathode dark space of hollow-cathode discharges has been detected and fully characterized. The complete understanding of the mechanisms that give rise to the signal is supported by a very good agreement between theoretical predictions and experimental results. Compactness and simplicity of the apparatus make this technique extremely attractive to study photoionization and its spectroscopic and analytical applications (resonance ionization spectroscopy).

ACKNOWLEDGMENTS

One of the authors (M.B.) expresses her gratitude for fruitful and stimulating discussions to Dr. P. K. Schenck, Dr. J. C. Travis, Dr. G. C. Turk, Dr. T. Berthoud, and Dr. P. Camus. Encouragement and fruitful cooperation by Dr. J. C. Travis is particularly appreciated and gratefully acknowledged. This work was performed (A.M.) in fulfillment of the requirements for a Ph.D.

APPENDIX

Analogously to the authors of Refs. 13 and 14, we could use the induced charge formalism[11] on the anode

$$q_A(t) = -eS \int_0^w \frac{x}{w}[n_i(x,t) - n_e(x,t)]dx - q_{x=w}(t) , \tag{A1}$$

$$i(t) = -\frac{dq_A(t)}{dt} , \tag{A2}$$

or on the cathode

$$q_C(t) = -eS \int_0^w \frac{w-x}{w}[n_i(x,t) - n_e(x,t)]dx - q_{x=0}(t) , \tag{A3}$$

$$i(t) = \frac{dq_c(t)}{dt} , \tag{A4}$$

where $q_{x=w}(t)$ and $q_{x=0}(t)$ are all the electrical charges which at time t have attained the anode and the cathode, respectively. Signs in Eqs. (A2) and (A4) have been set according to the selected positive current direction (cathode to anode).

In actuality, for computation purposes, it is more practical to use the following expressions:

$$j(t) = -\frac{1}{s}\frac{dq_A}{dt} = e\frac{d}{dt}\int_0^w \frac{x}{w}[n_i(x,t) - n_e(x,t)]dx + e[F_i(w,t) - F_e(w,t)] , \tag{A5}$$

$$j(t) = \frac{1}{s}\frac{dq_c}{dt} = -e\frac{d}{dt}\int_0^w \frac{w-x}{w}[n_i(x,t) - n_e(x,t)]dx + [F_i(0,t) - F_e(0,t)] , \tag{A6}$$

which are perfectly equivalent to (A1)–(A4). Full correspondence between Eqs. (A5), (A6), and (26) can be easily checked by replacing continuity equations (22) into the integrals of Eqs. (A5) and (A6) and integrating by parts. The flux term on the right-hand side in Eqs. (A5) and (A6) is the "real" current component mentioned by Berthoud *et al.* in Ref. 14.

---

[1] R. B. Green, R. A. Keller, G. G. Luther, P. K. Schenck, and J. C. Travis, Appl. Phys. Lett. 29, 727 (1976).

[2] K. C. Smith and P. K. Schenck, Chem. Phys. Lett. **55**, 466 (1978).

[3] C. Drèze, Y. Démers, and J. M. Gagné, J. Opt. Soc. Am. **72**, 912 (1982).

[4] A. Ben-Amar, G. Erez, and R. Shuker, J. Appl. Phys. **54**, 3688 (1983).

[5] M. Broglia, F. Catoni, and P. Zampetti, J. Phys. (Paris) Colloq. **44**, C7-479 (1983).

[6] G. Francis, *The Glow Discharge at Low Pressure,* in Vol. XXII of *Encyclopedia of Physics* (Springer, Berlin, 1956), pp. 53–208.

[7] R. A. Keller, B. E. Warner, E. F. Zalewski, P. Dyer, R. Engleman, Jr., and B. A. Palmer, J. Phys. (Paris) Colloq. **44**, C7-23 (1983).

[8] K. Kawakita, T. Nakajima, Y. Adachi, S. Maeda, and C. Hirose, Opt. Commun. **48**, 121 (1983).

[9] J. Blaise and L. J. Radziemski, Jr., J. Opt. Soc. Am. **66**, 644 (1976).

[10] G. S. Hurst, M. G. Payne, S. D. Kramer, and J. P. Young, Rev. Mod. Phys. **51**, 767 (1979).

[11] B. B. Rossi and H. H. Staub, *Ionization Chambers and Counters* (McGraw-Hill, New York, 1949), pp. 20–71.

[12] See, for instance, B. Chapman, *Glow Discharge Processes* (Wiley, New York, 1980) and references therein.

[13] P. K. Schenck, J. C. Travis, and G. C. Turk, J. Phys. (Paris) Colloq. **44**, C7-75 (1983).

[14] T. Berthoud, N. Drin, J. Lipinsky, and P. Camus, J. Phys. (Paris) Colloq. **44**, C7-67 (1983).

[15] J. C. Travis, G. C. Turk, J. R. De Voe, P. K. Schenck, and C. A. van Dijk, Prog. Anal. At. Spectrosc. **7**, 199 (1984).

[16] P. Cvitanović, *Universality in Chaos* (Hilger, Bristol, 1984), Part 4.

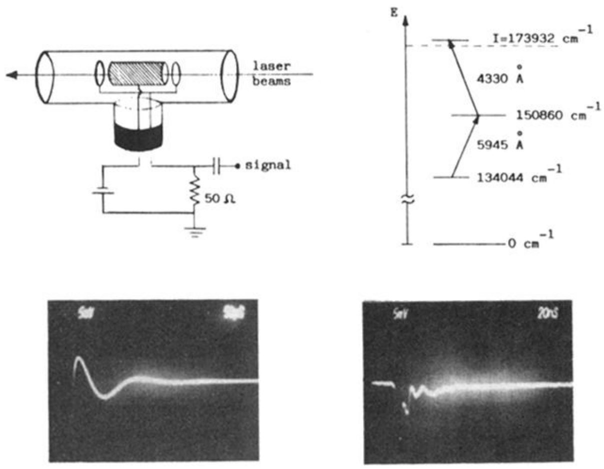

FIG. 2. Detected electrical signal produced by two-step resonant photoionization of Ne $^3P_2(1s_5)$ in a see-through hollow-cathode discharge. The optogalvanic effect related to the first step (5945 Å) is visible in the μs range; when the second laser is switched on and tuned on an autoionizing state, a mere expansion of the oscilloscope time scale makes the fast photoionization signal evident. This signal is strictly dependent on both lasers tuning and strongly enhanced near the cathode walls.